

Unveiling the mechanism of attaining high fill factor in silicon solar cells

Hao Lin¹ | Genshun Wang^{1,2,3} | Qiao Su^{1,2,3} | Can Han¹ | Chaowei Xue^{2,3} | Shi Yin^{2,3} | Liang Fang^{2,3} | Xixiang Xu^{2,3} | Pingqi Gao¹

¹School of Materials, Institute for Solar Energy Systems, Shenzhen Campus of Sun Yat-sen University, No. 66, Gongchang Road, Shenzhen, Guangdong, 518107, China

²LONGi Green Energy Technology Co., Ltd., Xi'an, 710016, China

³LONGi Central R&D Institute, Xi'an, 712000, China

Correspondence

Pingqi Gao, School of Materials, Institute for Solar Energy Systems, Shenzhen Campus of Sun Yat-sen University, No. 66, Gongchang Road, Shenzhen, Guangdong 518107, China.
 Email: gaopq3@mail.sysu.edu.cn

Funding information

Guangdong Basic and Applied Basic Research Foundation, Grant/Award Number: 2019B151502053; National Key Research and Development Program of China, Grant/Award Number: 2022YFB4200203; National Natural Science Foundation of China, Grant/Award Numbers: 62104268, 62034009; Shenzhen Fundamental Research Program, Grant/Award Number: JCYJ20200109142425294

Abstract

A world record conversion efficiency of 26.81% has been achieved recently by LONGi team on a solar cell with industry-grade silicon wafer (274 cm², M6 size). An unparalleled high fill factor (FF) of up to 86.59% has also been certified in a separated device. The theoretical FF limit has been predicted to be 89.26%, while the practical FF is far below this limit for a prolonged interval due to the constraints of recombination (i.e., SRH recombination) and series resistance. The ideality factor (*m*) in the equivalent circuit of silicon solar cells is consistently ranging from 1 to 2 and rarely falls below 1, resulting in a relatively lower FF than 85%. Here, this work complements a systematic simulation study to demonstrate how to approach the FF limit in design of silicon solar cells. Firstly, a diode component with an ideality factor equal to 2/3 corresponding to Auger recombination is incorporated in the equivalent circuit for LONGi ultra-high FF solar cell; Secondly, an advanced equivalent circuit is put forward for comprehensive analysis of bulk recombination and surface recombination on the performance, in which specific ideality factors are directly correlated with various recombination mechanisms exhibiting explicit reverse saturation current density (J_0). Finally, we evaluate precisely the route for approaching theoretical FF in practical solar cell fabrication based on electrical design parameters using the developed model.

KEY WORDS

diode model, fill factor, recombination, silicon solar cell

1 | INTRODUCTION

The current density–voltage (*J*-*V*) curve of conventional p-n junction usually satisfies the diode equation, $J_m = J_{0m}[\exp(V/(m \cdot V_{th})] - 1$, where J_{0m} , V_{th} , and m represent the reverse saturation current density, thermal voltage, and ideality factor, respectively. In most devices, the m value is ranging from 1 to 2, therefore equivalent circuit with

double diodes (with $m = 1$ and $m = 2$) is widely used for more precise description of the *J*-*V* characteristics. This double-diode model serves as core methodology in analytical models or softwares in silicon photovoltaic (PV), such as minority charge carrier analysis of surface recombination (reverse saturation current density, J_0) by Sinton,¹ carrier selectivity model by Brendel et al.,^{2,3} equivalent circuit,⁴ and Griddler software.⁵

This is an open access article under the terms of the [Creative Commons Attribution-NonCommercial-NoDerivs](#) License, which permits use and distribution in any medium, provided the original work is properly cited, the use is non-commercial and no modifications or adaptations are made.

© 2024 The Authors. Progress in Photovoltaics: Research and Applications published by John Wiley & Sons Ltd.

The intrinsic recombination in crystalline silicon (c-Si) bulk is intrinsically dominated by Auger rather than radiative process by its indirect bandgap nature. In the development of c-Si solar cell, the extrinsic recombination, that is, defective bulk and surface recombination, normally limits cell performance and covers up the Auger recombination effect. As such in an equivalent circuit for c-Si solar cell, the Auger recombination containing information of $J_{0\ 2/3}$ (reverse saturation current density with $m = 2/3$)⁶ only reveals itself when the defect-related recombination indicated by J_{01} and J_{02} (reverse saturation current density with $m = 1$ and 2, respectively) are suppressed to a substantially low level. Assuming defect-free fabrication processes (Auger recombination dominant), Richter et al estimated that a theoretical power conversion efficiency (PCE) and upper limit of FF for c-Si solar cells are 29.4% and 89.26%, respectively.⁷ In practical c-Si solar cell fabrication, the following electrical performances are demanded to approach the theoretical FF limit⁸: high-quality wafer (lifetime of SRH, $\tau_{SRH} > 10$ ms), low surface recombination ($J_{0\ surf} < 2$ fA/cm²), and low series resistance ($R_S < 0.2$ Ω·cm²). While wafer quality is improved continuously, surface passivation and series resistance become the major challenge to enhance c-Si solar cell performance to break the predicted limit of FF merely on J_{01} diode equation, that is, $FF = \sim 85\%$ of Green limit⁹ with $m = 1$. For examples, passivated emitter and rear cells (PERCs) and tunnel oxide passivated contact (TOPCon) solar cells with a diffused junction are inaccessible from perfect surface passivation, while silicon heterojunction (SHJ) solar cell is struggling in minimize the contact resistance.¹⁰ Recently, LONGI team broke the Green limit for FF of $m = 1$ by developing a p-type nanocrystalline silicon contact possessing ultra-low activation energy.¹¹ The simultaneous optimization of passivating contact ($J_{0\ surf} < 1.5$ fA/cm², contact resistance of $p_c < 20$ mΩ·cm²) and series

resistance ($R_S < 0.2$ Ω·cm²) leads to a world record FF of 86.59%.¹¹ In this context, it is critical to revisit the existing c-Si solar cell models, including the FF improvement strategy, the characterization of the m for recombination at different injection level, and the equivalent circuit model for recombination modeling.

In this study, we first demonstrate the measured J-V characteristics of the solar cell with record FF. The upward trend of FF along with surface recombination suppression is explained by double-diode model with J_{01} and $J_{0\ 2/3}$ (representing the surface recombination and Auger recombination, respectively). Subsequently, the correlation between the modified double-diode model and various recombination mechanisms are elucidated. A detailed description of the influence of bulk recombination and surface recombination, as well as the corresponding simplified J_0 , on cell performance is presented. Finally, two methods, that is, conventional equivalent circuit model and simplified recombination model, are established for accurate analysis and fit of the solar cell J-V parameters. The guideline for approaching theoretical FF limit is discussed.

2 | REALIZATION OF ULTRA-HIGH FF IN C-SI SOLAR CELL

Figure 1a shows the PCE of notable high-performance solar cells in relation to open circuit voltage (V_{OC}) and FF. The Green limit⁹ lines of $m = 2/3$ and $m = 1$ (gray dotted lines), as well as the two “intrinsic recombination + surface recombination” curves (blue and red solid lines) are given. The intrinsic recombination was calculated by using the Auger recombination model proposed by Black and Macdonald¹² and considering radiative recombination with a photon recycling

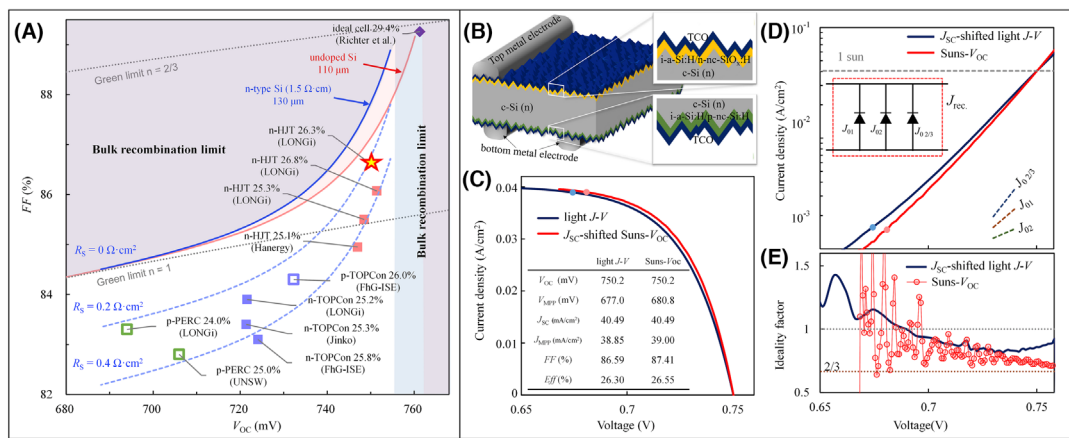


FIGURE 1 Realization of ultra-high FF in c-Si solar cell. (a) PCE of notable high-performance silicon solar cells in relation to V_{OC} and FF.¹¹ The blue and red solid lines are the $FF-V_{OC}$ curves calculated by only considering the bulk intrinsic recombination and the surface J_{01} recombination, and assuming a negligible series resistance (R_S), where blue and red solid lines represent the 130-μm-thick n-type (1.5 Ω·cm) wafer and 110-μm-thick undoped wafer, respectively. The areas colored by semitransparent blue/red represent the restricted region due to the bulk recombination limit. Blue dashed lines represent the $FF-V_{OC}$ curves (corresponding to the blue solid line) taking different R_S into account. (b-e) The structure diagram (b), J-V curves with liner ordinate (c), J-V curves with logarithmic ordinate (d), and m-V curves (e) for the silicon solar cell with record FF labeled by yellow star in (a). The light J-V curve is shifted by $-J_{SC}$ to obtain the “ J_{SC} -shifted light J-V” curve in (d), while the Suns- V_{OC} curve is shifted by $+J_{SC}$ to obtain the “ J_{SC} -shifted Suns- V_{OC} ” curve in (c). The inset in (d) is the equivalent circuit of the three diodes, while the three diagonal dashed lines at the bottom right represent the J-V curves' slope of those three diodes. The m-V curves were extracted from (d).

probability of 0.6¹³ (n-type c-Si wafer, 130 μm , 1.5 $\Omega\cdot\text{cm}$, and 110 μm , undoped c-Si), while the surface recombination is modeled by varying J_{01} . It shows clearly that the V_{OC} value is strongly promoted by advanced surface passivation from PERC (green square) to TOPCon (blue square) and then to SHJ (red square) cells. A rapid promotion of FF is observed at a transition point where V_{OC} exceeds 740 mV. For the LONGi's SHJ cells with V_{OC} of around 750 mV, the FF rapidly changes from $\sim 85\%$ to 86.6% at a relatively small increase of V_{OC} . The data points of different high-performance silicon solar cell are located between the two blue dashed lines marked by $R_S = 0.2 \Omega\cdot\text{cm}^2$ and $R_S = 0.4 \Omega\cdot\text{cm}^2$, indicating they obey the trend of “intrinsic recombination + surface recombination” curve but with R_S of 0.2–0.4 $\Omega\cdot\text{cm}^2$.

Figure 1b–e displays the information of the cell with record FF (yellow star in Figure 1a). As shown in Figure 1b, this n-type silicon solar cell featuring electron-selective contact of TCO/n-nc-SiO_x:H/i-a-Si:H and hole-selective contact of TCO/(p-nc-Si:H)/i-a-Si:H, where TCO, n-nc-SiO_x:H, p-nc-Si:H, and i-a-Si:H are transparent conducting oxide, n-type hydrogenated nanocrystalline silicon oxide, p-type hydrogenated nanocrystalline silicon, and intrinsic hydrogenated amorphous silicon, respectively. Three types of J-V curves¹⁴ are shown in Figure 1c–e, namely, J-V curves with linear y-axis (Figure 1c, usually describes the light J-V curve), J-V curves with logarithmic y-axis (Figure 1d, usually describes the dark J-V curve) and m-V curves (Figure 1e, derivative of the J-V curves in Figure 1d). In Figure 1c, the blue solid line represents the light J-V curve acquired from ISFH CalTech, in comparison to the Suns- V_{OC} curve (red solid line) obtained in our Lab. Inset table in Figure 1c summarizes the J-V

parameters derived from the above two curves. Series resistance effect is eliminated in Suns- V_{OC} measurement and explains the high FF. As shown in Figure 1d, the J-V curves of tree diodes with $m = 1$, $m = 2$ and $m = 2/3$ (colored dotted lines marked by J_{01} , J_{02} , and $J_{02/3}$) present different slopes, corresponding to the equivalent circuit in the inset. The actual J-V curve contains abovementioned information of tree diodes, which can be extracted by the slope of J-V curve. Figure 1e shows the m-V curves, where m is calculated by the equation of $m = 1/V_{\text{th}} \cdot (dV/d\ln J)$, representing the slope of J-V curves (Figure 1d) at difference voltage points. The curves of Suns- V_{OC} and J_{SC} -shifted light J-V basically follows the same trend for the voltage range below 740 mV. While the J_{SC} -shifted light J-V curve has a slight upward warping once the voltage exceeds 740 mV. This discrepancy is believed to be related to the series resistance. In addition, near the V_{OC} point, the m value is close to 2/3, indicating that the Auger recombination becomes dominant factor.

3 | EXPLANATION VIA A DOUBLE-DIODE MODEL WITH J_{01} AND $J_{02/3}$

A modified double-diode model is introduced to explain the “intrinsic recombination + surface recombination” curve in Figure 1a, where the diode J_{01} and diode $J_{02/3}$ represent the surface recombination and intrinsic recombination, respectively. Similar to Figure 1d, Figure 2a shows the J-V curves with logarithmic y-axis. According to the evaluation of intrinsic recombination of the wafer (130 μm , n-type c-Si, 1.5 $\Omega\cdot\text{cm}$), $J_{02/3}$ is set to $2.5 \times 10^{-21} \text{ A/cm}^2$, and its J-V curve is

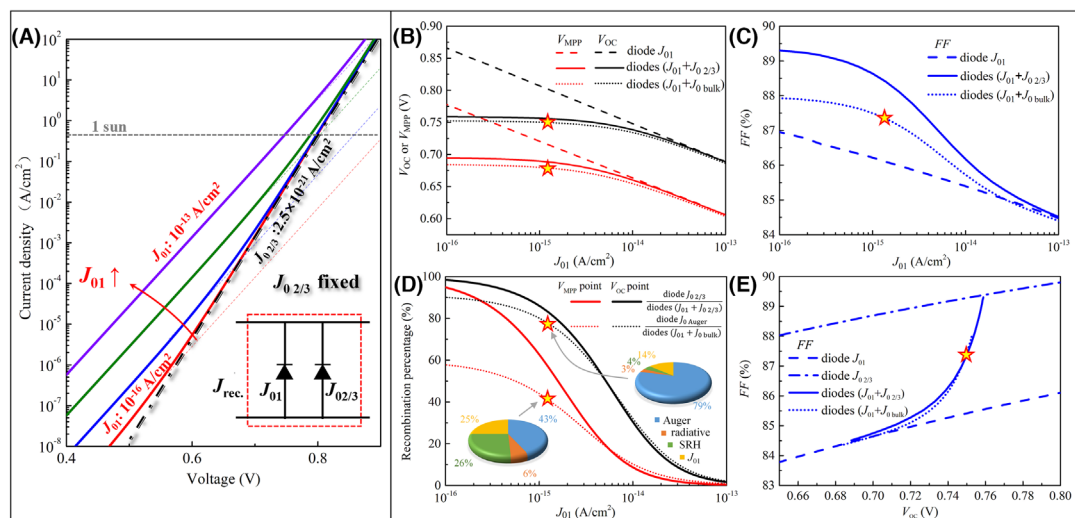


FIGURE 2 Exploration of the underlying mechanism for ultra-high FF using a double-diode model. (a) The J-V curves of double-diodes with J_{01} and $J_{02/3}$. The J_{01} ranges from 10^{-16} to 10^{-13} A/cm^2 , while the $J_{02/3}$ is fixed at $2.5 \times 10^{-21} \text{ A/cm}^2$. The inset is the equivalent circuit of the double diodes. The intersections of the colored lines with the gray dashed line of 1 sun indicate the V_{OC} under different J_{01} . (b–e) The PV parameters of single diode with J_{01} (labeled by diode J_{01}) and double diodes with J_{01} and $J_{02/3}$ (labeled by diodes $J_{01} + J_{02/3}$): (b) V_{OC} or V_{MPP} as a function of J_{01} ; (c) FF as a function of J_{01} ; (d) at V_{OC} or V_{MPP} point, recombination percentage of diode $J_{02/3}$ in diodes $J_{01} + J_{02/3}$ as a function of J_{01} ; (e) FF as a function of V_{oc} . The yellow stars represent the solar cell with record FF, while the curves marked by diode $J_{0\text{bulk}}$ or diode $J_{0\text{Auger}}$ (short dotted lines) represent the actual situation given by the simplified recombination model (Section 6). The pie charts in d are the detail recombination percentage of the record FF solar cell at V_{MPP} and V_{OC} points.

given by the black dot-dashed line, while the J - V curves of diode J_{01} (colored solid and extended dotted lines) are shifted from the bottom right to the upper left (red arrow) with the increase of J_{01} from 10^{-16} to 10^{-13} A/cm^2 . The double diodes are set in parallel (inset) so that the total recombination current density equals to the sum of the intrinsic and surface components. Because the slope of J - V curve of diode J_{01} is smaller than that of diode $J_{0\ 2/3}$, the J_{01} diode information only manifests within a certain range of voltages below a transition point, while this transition voltage (the dividing point dominated by diode J_{01} and diode $J_{0\ 2/3}$) is moving up from ~ 0.6 to $> 0.9 \text{ V}$ with the growth of J_{01} from 10^{-16} to 10^{-13} A/cm^2 . As a consequence of increasing J_{01} , the information of $J_{0\ 2/3}$ diode within the voltage range of V_{MPP} – V_{OC} (V_{MPP} is voltage at maximum power point) will gradually submerge under that of J_{01} diode. FF basically obeys the curve rule of diode with J_{01} (i.e., Green limit $m = 1$ in Figure 1a) when J_{01} above 10^{-14} A/cm^2 and gradually transits to comply with Green limit $m = 2/3$ as J_{01} is suppressed, especially when down to 10^{-16} A/cm^2 . From the point of view of V_{OC} and V_{MPP} , above phenomenon of rapid increase in FF with the decline of J_{01} can be better described in Figure 2b–e. In terms of FF, the electrical component V_{MPP}/V_{OC} plays a more important role than the optical component J_{MPP}/J_{SC} , and thus, the V_{MPP} and V_{OC} as a function of J_{01} is presented in Figure 2b. For single diode J_{01} , the V_{MPP} (or V_{OC}) will increase linearly (dashed lines) with the decrease of J_{01} , leading to a similar trend of linear increase in FF (dashed line in Figure 2c). For diodes $J_{01} + J_{0\ 2/3}$, with the decrease of J_{01} , one can see the V_{MPP} (or V_{OC}) enters into a saturation voltage of $\sim 695 \text{ mV}$ (or $\sim 760 \text{ mV}$) (limited by fixed $J_{0\ 2/3}$). Because the changing point of V_{OC} entering into the saturation range is prior to that of V_{MPP} , that is, $J_{01} \sim 8 \text{ fA/cm}^2$ versus $J_{01} \sim 1 \text{ fA/cm}^2$ (solid lines in Figure 2d), leading to a rapid increase of FF during the decrease of J_{01} of 10^{-14} – 10^{-15} A/cm^2 (solid line in Figure 2c). Finally, according to Figure 2b and Figure 2c, the curves of FF as a function of V_{OC} can be plotted with canceling out the intermediate variable of J_{01} , as shown in Figure 2e. Therefore, with the continuous increase of V_{OC} , embodying that the proportion of surface recombination significantly decreases and more intrinsic recombination information related to $J_{0\ 2/3}$ is revealed, FF therefor changes from original dashed line (diode J_{01}) to the dot-dashed line (diode $J_{0\ 2/3}$).

The solar cell with record FF is also marked by yellow stars in Figure 2b–e, and the corresponding parameters have a little deviation from the curves of diodes $J_{01} + J_{0\ 2/3}$. Obviously, using diode $J_{0\ 2/3}$ is too simple to describe the actual situation. In fact, the diode $J_{0\ 2/3}$ should be replaced by recombination of silicon bulk (marked by diode $J_{0\ bulk}$) including Auger, radiative, and Shockley–Read–Hall (SRH) recombination, which will be discussed in the next section. While from the curves considering real recombination (dotted lines) marked by diodes $J_{01} + J_{0\ bulk}$, those show similar trends as above situation of only considering diodes $J_{01} + J_{0\ 2/3}$. As show in Figure 2d, the percentage of Auger recombination (marked as diode $J_{0\ Auger}$) in total recombination reached at 43% and 79% for V_{MPP} and V_{OC} points, indicating the FF surpass over 86% dominated by Auger recombination has appeared. It should mention that $J_{0\ 2/3}$ only correlates the information of J_0 with $m = 2/3$, a unique character of Auger recombination

TABLE 1 The formula of recombination rate (U) corresponding to radiative, Auger, and Shockley–Read–Hall (SRH) recombination, where B , C_n^* , and C_p^* are the coefficients of radiative recombination, electron Auger recombination, and hole Auger recombination, respectively. The n_i , n , and p are the concentration of intrinsic carrier, electron, and hole, respectively. The τ_{p0} and τ_{n0} are the wafer-quality dependent hole and electron capture time constant, respectively. The n_1 (p_1) is the Shockley–Read factor for electrons (holes), which depends on the location of trap level and can be ignored when it closes to the E_i (i.e., defects of deep level). Δn and N_D are the excess carrier concentration and doping concentration of silicon bulk, respectively. The analysis of U_{SRH} at low (or high) injection is simplified under assumption of $\tau_{n0} = \tau_{p0} = \tau_{SRH}$ and deep level located trap.

| | U_{rad} | U_{Auger} | U_{SRH} |
|--|------------------------|--|---|
| Formula | Bnp | $C_n^* n^2 p + C_p^* np^2$ $\frac{(np - n_1^2)}{\tau_{p0}(n+n_1) + \tau_{n0}(p+p_1)}$ | |
| Low injection ($\Delta n \ll N_D$) | $BN_D \cdot \Delta n$ | $C_n^* N_D^2 \cdot \Delta n$ | $\frac{1}{\tau_{SRH}} \Delta n$ |
| High injection ($\Delta n \gg N_D$) | $B \cdot (\Delta n)^2$ | $(C_n^* + C_p^*) (\Delta n)^3$ | $\frac{1}{2 \cdot \tau_{SRH}} \Delta n$ |

at high injection. However, in fact, the m and J_0 of real Auger recombination will change along with the voltage, so using $J_{0\ Auger}$ to represent the calculated Auger recombination is more accuracy than $J_{0\ 2/3}$. In general, $J_{0\ Auger}$ includes $J_{01\ Auger}$ and $J_{0\ 2/3\ Auger}$, which will be discussed in next part.

4 | CORRELATIONS BETWEEN RECOMBINATION AND DIODE MODEL

The diode model is strongly correlated with the recombination model. For the ideal silicon solar cell, the quasi-Fermi level across all regions in bulk is assumed as same, and thus, the implied V_{OC} (iV_{OC} , i.e., the difference between the two quasi-Fermi level for electrons and holes) equals to the applied voltage (more details are showed in Figure S1). According to the equation of $J_{rec.} = UqW_{bulk}$, the characteristics of J - V curve in device is similar as that of U - iV_{OC} curve, where $J_{rec.}$, U , q , and W_{bulk} are the recombination current density, recombination rate, electron charge, and the thickness of bulk, respectively.¹⁵ Therefore, comprehension of the characteristics of U - iV_{OC} curves with variable recombination in bulk, and the contribution of U to the diode model of J_{01} , J_{02} , and $J_{0\ 2/3}$ contributes to interpretation of the characteristics of J - V curves in real devices.

Formulas for recombination rate (i.e., U_{rad} , U_{Auger} , and U_{SRH} , respectively) of radiative recombination, Auger recombination, and Shockley–Read–Hall (SRH) recombination are listed in Table 1. In the formulas, n and p represent the carrier concentration of electron and hole, respectively. The difference in their product indicates different number of particles involved in a recombination process. For examples, radiative recombination with U proportional to np associates a two-particle process, while Auger recombination with U proportional to n^2p associates a three-particle process. The SRH recombination is

an intermediate-defect-state assisted two-particle process resulting in a formula more complex than the other two. To reveal subtle among the differences, the expressions of U are analyzed in separate situations of low injection and high injection. Under low injection condition, the excess carrier concentration (Δn) is much lower than the doping concentration (N_D) of silicon bulk, that is, $\Delta n \ll N_D$. The high injection condition is vice versa. The corresponding variables and constants are expressed in red and black fonts, respectively. Under low injection, the recombination rate U follows the change of Δn linearly for all recombination processes (the second row in Table 1). The Δn and iV_{OC} dependence satisfies the following equation at low injection.

$$\Delta n = \frac{n_i^2}{N_D} \cdot \exp\left(\frac{iV_{OC}}{1V_{th}}\right) \quad (1)$$

which means the ideality factor for all recombination rates is 1 (i.e., $m = 1$) at low injection, where n_i , iV_{OC} , and V_{th} are intrinsic carrier concentration (silicon bulk), implied V_{OC} , and thermal voltage, respectively.

Under high injection, the recombination rate U follows the change of Δn to the second, third, and first power depending on the recombination process. Considering high injection, Δn is the exponential increase function of iV_{OC} with an ideality factor of 2, that is,

$$\Delta n = n_i \cdot \exp\left(\frac{iV_{OC}}{2V_{th}}\right) \quad (2)$$

Therefore, under high injection, the ideality factors corresponding to radiative recombination, Auger recombination and SRH recombination are 1, 2/3, and 2, respectively. In fact, from Equations (1) and (2), the Δn increases exponentially with the growth of iV_{OC} , for ideality factor $m = 1$ at low injection, and ideality factor $m = 2$ at high injection. The physical meaning is related to the relationship between the movement of the quasi-Fermi level and iV_{OC} (Figure S2). The change of iV_{OC} almost completely acts on the movement of minority carrier quasi-Fermi levels at low injection, while the movement values of the two quasi-Fermi levels are same and occupy half of the change of iV_{OC} at high injection.

Figure 3a–c shows the U - iV_{OC} curves of three types of recombination at different bulk doping concentrations (N_D). By extracting the slope of the U - iV_{OC} curves in logarithmic y-axis, one can get the m - iV_{OC} curves (Figure 3d–f) as well as the color diagrams of the m as a function of N_D and iV_{OC} (Figure 3g–i). As shown in Figure 3a,b, the low/high injection region can be well distinguished from the slope change of U - iV_{OC} curves. For SRH or Auger recombination, at low injection, the curve slope is $m = 1$ (marked as $J_{01 SRH}$ or $J_{01 Auger}$), while at high injection, the slope is $m = 2$ ($J_{02 SRH}$) or $m = 2/3$ ($J_{02 Auger}$).

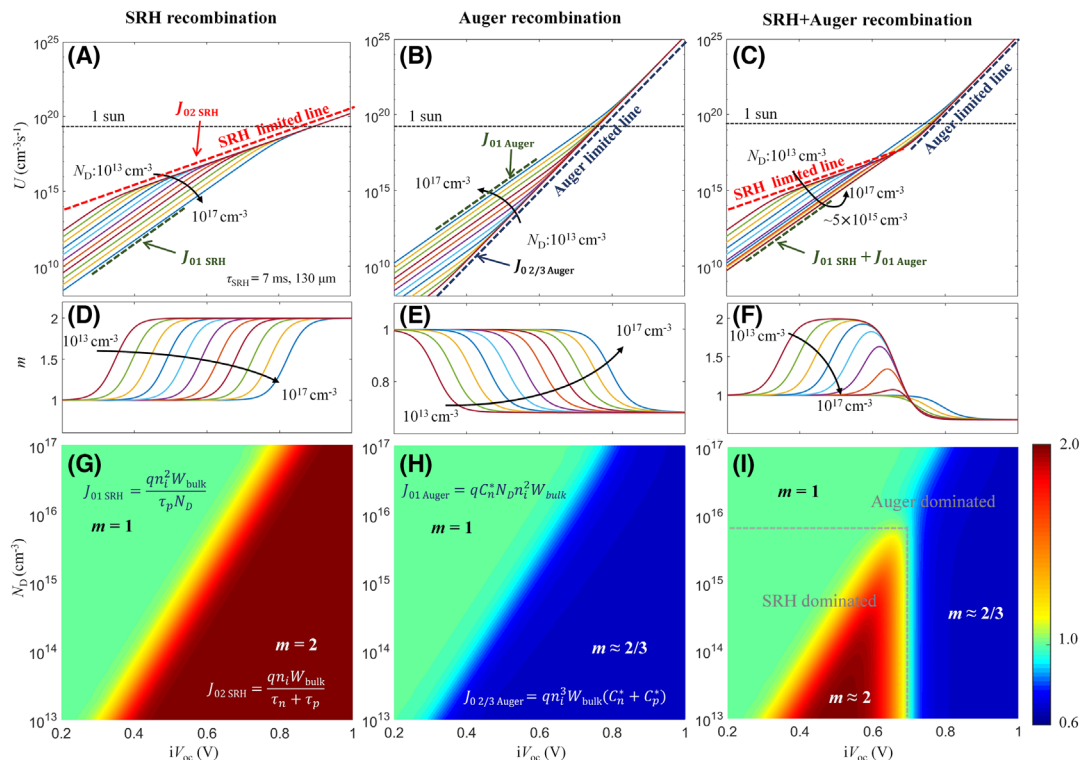


FIGURE 3 Recombination analysis. Recombination rate (U) (a–c) and ideality factor (m) (d–f) as a function of iV_{OC} with different N_D . (g–i) The color diagrams of m as a function of N_D and iV_{OC} , corresponding to SRH recombination, Auger recombination, and SRH + Auger recombination, from left to right. The lifetime of SRH recombination (τ_{SRH}) and the thickness of wafer (W_{bulk}) are separately set as 7 ms and 130 μ m. The one-sun line (black dotted line) is calculated by J_{SC}/qW_{bulk} , where the J_{SC} is set as 43.36 mA/cm 2 . The formulas indicated in (g) and (h) are that for calculating the recombination of J_0 in a and b. The radiative recombination (Figure S3) shows negligible influence on the final trend of recombination.

Auger). And the transition region in iV_{OC} of low/high injection increase from ~ 0.3 to ~ 0.8 V with the growth of N_D from 10^{13} to 10^{17} cm^{-3} , consistent with the definition of low/high injection in Table 1. This transition region can also be well observed in $m\text{-}iV_{\text{OC}}$ curves (in Figure 3d,e), that is, the region where m changed from 1 to 2 (from 1 to 2/3) for SRH (Auger) recombination. As $J_{01 \text{ SRH}} \propto 1/N_D$ and $J_{01 \text{ Auger}} \propto N_D$ (the formula showed in Figure 3g,h), the $J_{01 \text{ SRH}}$ and $J_{01 \text{ Auger}}$ showed opposite changes with the increase of N_D (direction of black arrows). On the other hand, Figure 3g,h shows that $J_{02 \text{ SRH}}$ and $J_{02/3 \text{ Auger}}$ is independent of N_D (labeled as the SRH limited line and Auger limited line), representing an upper limit of SRH recombination and a lower limit of Auger recombination, respectively. According to the formula of $J_{02 \text{ SRH}}$ and $J_{02/3 \text{ Auger}}$ inserted in Figure 3g,h, the upper limit of SRH is determined by τ_{SRH} and the thickness of bulk (W_{bulk}), while the lower limit of Auger is only determined by W_{bulk} . As shown in Figure 3c, when SRH and Auger are combined together, the $U\text{-}iV_{\text{OC}}$ curves become more complex. The dominant recombination

changes from $J_{01 \text{ SRH}}$ to $J_{01 \text{ Auger}}$ when the N_D increases. This explains why the combined U decreases first with higher N_D but turns around up when N_D increases further (black arrow). The figure of $m\text{-}iV_{\text{OC}}$ may help us distinguish the dominant recombination at different injection levels. As shown in Figure 3f, with low N_D , such as 10^{13} cm^{-3} , the dominated recombination current density is shifted from $J_{01 \text{ SRH}}$ ($m = 1$) to $J_{02 \text{ SRH}}$ ($m = 2$) and finally to $J_{02/3 \text{ Auger}}$ ($m = 2/3$). At higher N_D up to 10^{17} cm^{-3} , the corresponding $m\text{-}iV_{\text{OC}}$ curve is basically consistent with that of Auger recombination.

The color diagrams of the m are shown in Figure 3g,h. For example, in SRH (or Auger) recombination, the green region represents the J_{01} region of SRH (or Auger) recombination, that is, the low injection region, while the red (or blue) region represents the J_{02} (or $J_{02/3}$) region of SRH (or Auger) recombination, that is, the high injection region. In Figure 3i, the regions dominated by SRH recombination and Auger recombination can be quickly distinguished (the boundary is labeled with white dashed line). Due to the negligible effect of radiation

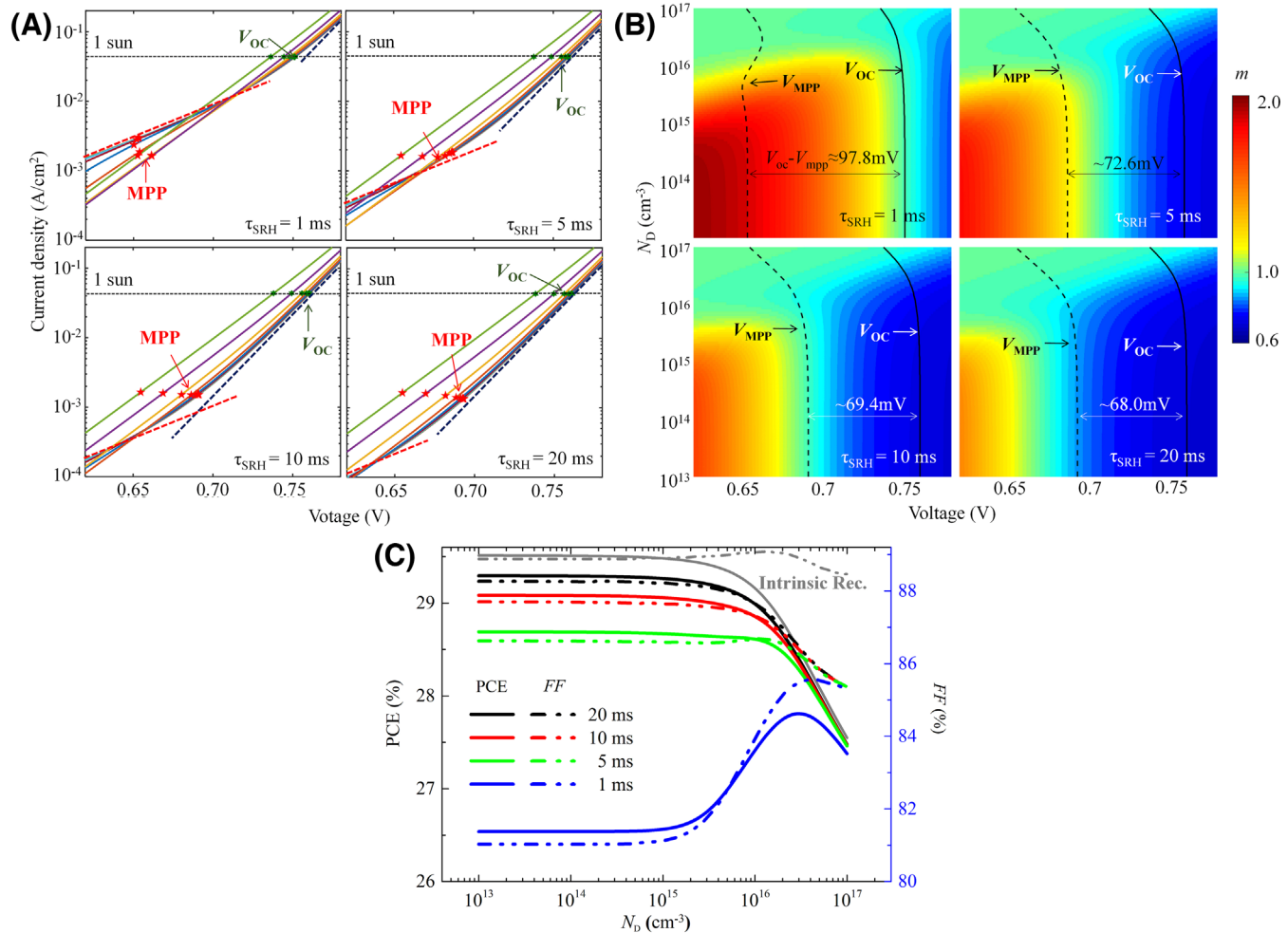


FIGURE 4 Bulk recombination. (a) The $J\text{-}V$ curves with four different lifetimes τ_{SRH} of the silicon wafers, where the different color lines are with different doping concentration (same as Figure 3c). The intersection point of $J\text{-}V$ curve and 1 sun line (black dotted line) is the corresponding V_{OC} . The red star represents its maximum power point (MPP), which is calculated by assuming a J_{SC} of 43.36 mA/cm^2 . The red and blue dashed lines represent the SRH and auger limited lines (similar as that in Figure 3a,b), respectively. (b) The color diagrams of ideality factor (m) as a function of doping concentration (N_D) and voltage at τ_{SRH} of 1, 5, 10, and 20 ms. the black dotted line and black solid line represent the V_{MPP} and V_{OC} , respectively. (c) The PCE and FF as a function of N_D for the four different τ_{SRH} .

recombination, the models of “Auger + radiative recombination” and “SRH + Auger + radiative recombination” are only presented in Figure S3 as supplements. Meanwhile, three-dimensional diagrams of above recombination containing more details are presented in Figure S4.

5 | QUANTIFICATION OF BULK AND SURFACE RECOMBINATION

Four kinds of wafers with different τ_{SRH} across a wide range from 1 to 20 ms were set to investigate the influence of wafer quality on solar cell performance. Figure 4a,b shows the J-V curves (assuming a $J_{\text{SC}} = 43.36 \text{ mA/cm}^2$) and the color diagrams of m as a function of V and N_{D} , respectively. The maximum power point (MPP) and V_{OC} are marked. One can readily perceive the impact of SRH recombination on MPP and V_{OC} point. For example, when $\tau_{\text{SRH}} = 1 \text{ ms}$, the SRH limited line (red dotted line) is above the MPP in Figure 4a, and V_{MPP} line is basically covered by red color representing SRH recombination with $m = \sim 2$ in Figure 4b. As such, the V_{MPP} point is more affected by the SRH recombination. With the increase of τ_{SRH} , the influence of SRH recombination on cell performance will be less pronounced, which is reflected by the downward moving of SRH limited line in Figure 4a, and the shrinking of SRH dominated region (red region) in Figure 4b. When τ_{SRH} surpasses 20 ms, the V_{MPP} line is basically covered by blue color. The J-V curve ranging from $V_{\text{MPP}}-V_{\text{OC}}$ is dominated by intrinsic recombination and FF approaches the theoretical limit. The increase of FF can also be reflected by the decreased span between V_{MPP} line and V_{OC} line in Figure 4b, from 97.8 to 68 mV, similar as that in Figure 2b.

Figure 4c shows the PCE and FF as a function of N_{D} under the four different τ_{SRH} (and the gray lines represent the situation with only considering intrinsic recombination, i.e., $\tau_{\text{SRH}} = \infty$). A perfect surface passivation and a fixed J_{SC} of 43.36 mA/cm^2 is assumed here. The PCE trending complies with that of FF, indicating that FF is the primary factor for PCE improvement when perfect surface passivation can be obtained. For a good quality wafer ($\tau_{\text{SRH}} \geq 5 \text{ ms}$), with the increase of N_{D} , the PCE and FF are independent of N_{D} at first and then deteriorate rapidly at a N_{D} higher than 10^{15} cm^{-3} where Auger recombination takes over. For a poor quality wafer ($\tau_{\text{SRH}} = 1 \text{ ms}$), with the growth of N_{D} , the PCE and FF also maintain a stable value at first, but followed by a rapid ramp up and down. The MPP point is primarily affected by $J_{02 \text{ SRH}}$ (independent of N_{D}) at low N_{D} , and then by $J_{01 \text{ SRH}} (\propto 1/N_{\text{D}})$ with at higher N_{D} , especially $N_{\text{D}} \geq 5 \times 10^{15} \text{ cm}^{-3}$, and finally by $J_{01 \text{ Auger}} (\propto N_{\text{D}})$. This leads to a practical guideline for solar cell fabrication on unsatisfactorily controlled wafer quality, in which scenario appropriately increasing the doping concentration of silicon wafers can help to obtain a higher PCE in more steady production.

The surface recombination velocity (S) describes the recombination severity of electron and hole at surface. The surface recombination rate (U_s) is defined as

$$U_s = S \cdot \Delta n_s \quad (3)$$

where Δn_s denotes excess carrier concentration at surface. We reveal here that surface field passivation plays a critical role in surface recombination due to its impact on surface excess carrier concentration. In the absence of a field, known as flat band state, the excess carrier concentration in the bulk is equal to that at the surface (i.e., $\Delta n = \Delta n_s$). In the presence of a field, a band bending forms in surface region making $\Delta n \neq \Delta n_s$.

Figure 5 shows the analysis of surface recombination under field passivation. The classic p+n junction is taken as an example here, while the field caused by the surface charge or the heterojunction with doped layer should have similar properties.

Figure 5a,b shows the schematic diagram of the band structure with two types of surface field (strong and weak) under the equilibrium state and nonequilibrium state, respectively. The φ_{s0} represents the barrier height of the surface, which is dependent on the doping concentration of the doped layer (N_{A+}) and silicon bulk (N_D). It can be expressed as

$$\varphi_{s0} = \beta \ln \left(\frac{p_{s0}}{p_0} \right) = \beta \ln \left(\frac{N_{A+}}{n_i^2 / N_D} \right) \quad (4)$$

where $\beta = kT/q$, with the Boltzmann constant k , the absolute temperature T , and the electron charge q . A linear dependence of φ_{s0} on $\ln(N_{A+})$ is thus revealed here. With the increase of iV_{OC} , as shown in Figure 5a,b (right panels), the surface field φ_s will decrease. It satisfies $\varphi_s = \varphi_{s0} - iV_{\text{OC}}$ at low injection ($\Delta n \ll N_D$) and $\varphi_s = (\varphi_{s0} - iV_{\text{OC}})/2$ at high injection ($\Delta n \gg N_D$) (Figure S5). Because of high φ_{s0} (high N_{A+} ; Figure 5a), it can keep low injection ($\Delta n_s < N_{A+}$) at surface, making the surface recombination dominated by J_{01} (marked as $J_{01 \text{ surf}}$) at the range below V_{OC} . For low N_{A+} at surface, weak bend banding of φ_{s0} (Figure 5b) is formed and makes the surface to quickly enter the high injection ($\Delta n_s > N_A$), mainly leading to the surface recombination J_{02} ($J_{02 \text{ surf}}$). At the edge of the p-n junction, low N_{A+} can be easily formed, which endows the edge a main source of $J_{02 \text{ surf}}$ (Figure S6).

Figure 5c shows the surface recombination rate (U_s/W_{bulk}) as a function of iV_{OC} . The formula for calculating the surface recombination rate (U_s) is

$$U_s = (n_s p_s - n_i^2) \int_{E_V}^{E_C} \frac{\nu_{\text{th}} D_{\text{it}}(E) dE}{\sigma_p^{-1}(E)[n_s + n_1(E)] + \sigma_n^{-1}(E)[p_s + p_1(E)]} \quad (5)$$

It assumes that the defects are mainly concentrated in deep level. The n_1 and p_1 are small values, the surface defect density of states $D_{\text{it}} = N_{\text{it}}(E - E_t)$, where N_{it} is the surface density at local energy level. The n_s and p_s are the electron and hole concentrations at the surface. The σ_p , σ_n , and ν_{th} are the hole capture cross section, electron capture cross section, and thermal velocity. E is the energy relative to the intrinsic energy. The corresponding formula (5) can be simplified as

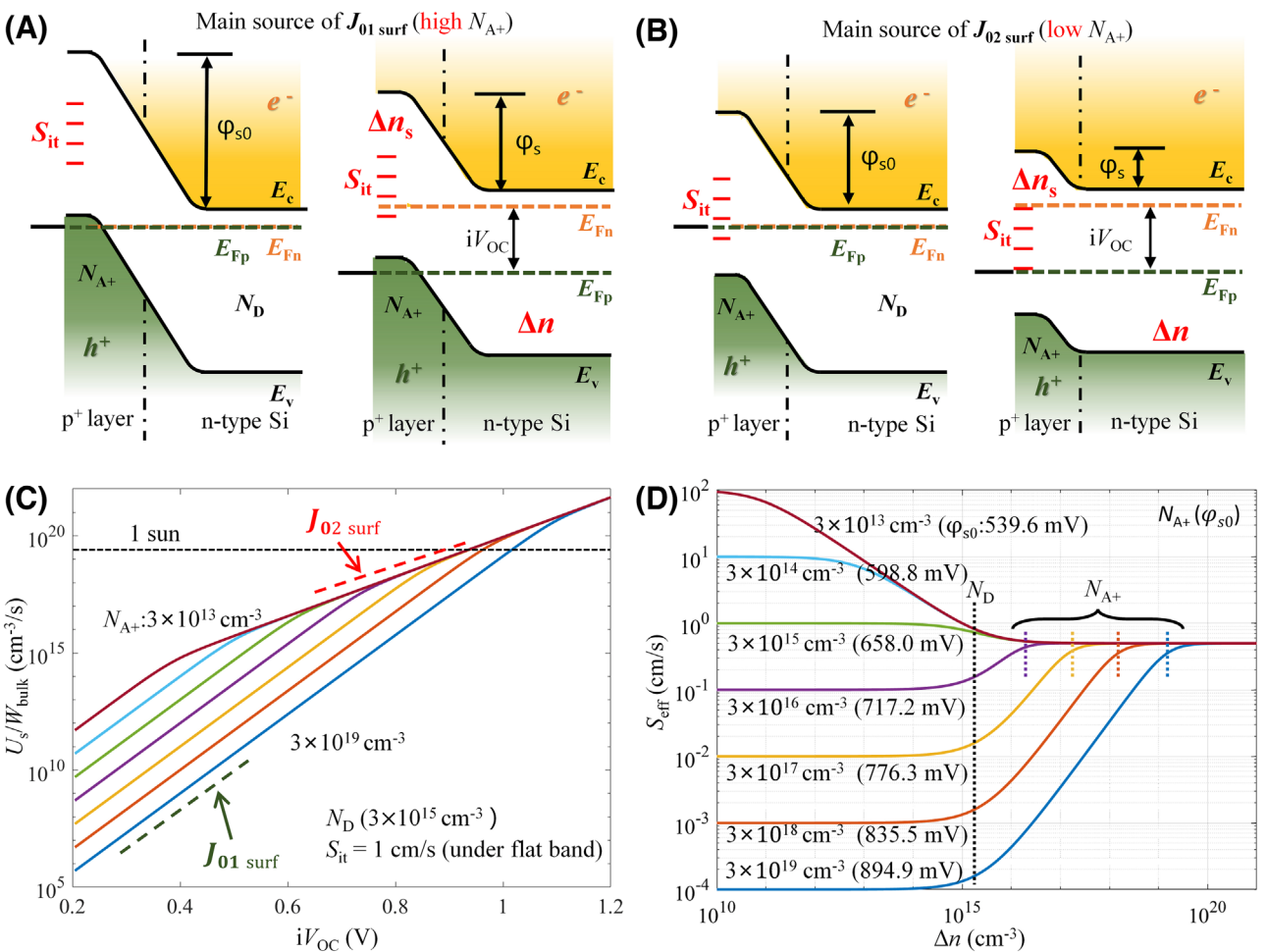


FIGURE 5 Surface recombination. (a,b) The schematic band structure diagrams of forming the surface recombination J_{01} ($J_{01\text{surf}}$) and surface recombination J_{02} ($J_{02\text{surf}}$) in the cases of strong field passivation (a, high N_{A+}) and weak field passivation (b, low N_{A+}), respectively. The band structure diagrams include the situation under the equilibrium state (left) and nonequilibrium state (right). Here, N_{A+} represents an effective p-type doping concentration at bulk surface, which can be formed by p+-doped layer, surface negative charge, and the heterojunction with p+-doped layer, while N_D is the doping concentration of bulk. S_{it} represents the surface recombination caused by defects. The φ_{s0} and φ_s are the surface barrier heights under equilibrium and nonequilibrium states, respectively. Δn_s and Δn are excess carrier concentrations at the surface and in the bulk, respectively. E_C , E_V , E_{Fn} , and E_{Fp} denote conduction band energy, valence band energy, electron quasi-Fermi level, and hole quasi-Fermi level, respectively. (c) The recombination rate from surface (U_s/W_{bulk}) as a function of iV_{OC} under different N_{A+} (representing the field passivation). The situations of low N_{A+} and high N_{A+} present J_{02} and J_{01} dominated information, respectively, at $V_{\text{MPP}}-V_{OC}$ range. (d) The effective surface recombination velocity (S_{eff}) as a function of Δn under different N_{A+} . Here, the surface recombination is introduced on the surface of the p⁺ layer, while S_{eff} represents the recombination rate caused by the surface defects with different field passivation. We set $S_{it} = 1 \text{ cm/s}$ as the case of chemical passivation (under flat band). The bulk silicon is n-type with an N_D of $3 \times 10^{15} \text{ cm}^{-3}$.

$$U_s \approx \frac{n_s p_s - n_i^2}{S_{p0}^{-1} n_s + S_{n0}^{-1} p_s} \quad (6)$$

The S_{p0} and S_{n0} are the hole and electron surface recombination velocities, where $S_{p0}^{-1} = v_{\text{th}} \sigma_p N_{it}$, $S_{n0}^{-1} = v_{\text{th}} \sigma_n N_{it}$.

It should be noted that the unit of U_s is $\text{cm}^{-2} \text{s}^{-1}$, so if U_s is compared with the previous recombination rate from bulk (like U_{Auger} or U_{SRH}), it needs to be divided by the wafer thickness of W_{bulk} , that is, U_s/W_{bulk} . Same as the SRH recombination in bulk (Figure 3a), at low injection ($\Delta n \ll N_{A+}$), the ideality factor of $m = 1$ and $J_{01\text{surf}} = (n_i^2/N_{A+})qS$, while at high injection ($\Delta n \gg N_{A+}$), $m = 2$, and $J_{02\text{surf}} = n_i q S$. The U_s/W_{bulk} will decrease with the growth of N_{A+} ,

and the curves dominated by J_{01} at $V_{\text{MPP}}-V_{OC}$ range when $N_{A+} > 3 \times 10^{17} \text{ cm}^{-3}$ (yellow line). In addition, under high injection, $U_s/W_{\text{bulk}}-iV_{OC}$ curves will also fall into a line with $m = 2$, and the curves will be dominated by J_{02} at $V_{\text{MPP}}-V_{OC}$ range when $N_{A+} < 3 \times 10^{14} \text{ cm}^{-3}$ (bright blue line).

To compare with the recombination in bulk, it is preferred to convert Δn_s in Equation (3) to Δn . From the definition of $S \cdot \Delta n_s = S_{\text{eff}} \cdot \Delta n$, and the assumption of $n_s p_s = np$ (i.e., the quasi-Fermi level keeps same at the surface and in bulk, and the n and p are the carrier concentration of electron and hole in bulk, while n_s and p_s are those at surface), the following equation can be deduced.

TABLE 2 Summary of the source of J_{01} , J_{02} , and $J_{0\ 2/3}$. The situation of the parameters under low (or high) injection was labeled as $_{\text{li}}$ (or $_{\text{hi}}$) at the subscript, such as $J_{0\ \text{Auger_hi}}$ (instead of the $J_{0\ 2/3\ \text{Auger}}$ above). R and J_0 represent the amount of recombination and the reverse saturation current density, respectively. W and N are the thickness and doping concentration of different layers, respectively.

| R | Ideality factor (m) | Rec. type | Rec. formula | Rec. area | J_{0m} |
|--|-------------------------|--|--|----------------------|--|
| $\approx R_{02/3} \left(\frac{pn}{n_i^2} \right)^{3/2}$ | 2/3 | Auger Rec. in high injection | $R_{\text{Auger_hi}} \approx (C_n^* + C_p^*) W_{\text{bulk}} \Delta n^3$ | Bulk | $J_{0\ \text{Auger_hi}} = qn_i^3 W_{\text{bulk}} (C_n + C_p)$ |
| $\approx R_{01} \left(\frac{pn}{n_i^2} \right)^{2/2}$ | 1 | Radiative Rec. (band to band) | $R_{\text{rad}} \approx BW_{\text{bulk}} pn$ | Bulk | $J_{0\ \text{rad}} = qBn_i^2 W_{\text{bulk}}$ |
| | | Auger Rec. in low injection | $R_{\text{Auger_li_p+}} \approx C_p^* N_{A+} W_{p+} pn$ | p+ | $J_{0\ \text{Auger_li_p+}} = qC_p^* N_{A+} n_{i(\text{eff})}^2 W_{p+}$ |
| | | | $R_{\text{Auger_li_n+}} \approx C_n^* N_{D+} W_{n+} pn$ | n+ | $J_{0\ \text{Auger_li_n+}} = qC_n^* N_{D+} n_{i(\text{eff})}^2 W_{n+}$ |
| | | | $R_{\text{Auger_li_p}} \approx C_p^* N_A W_{\text{bulk}} pn$ | Bulk (p) | $J_{0\ \text{Auger_li_p}} = qC_p^* N_A n_i^2 W_{\text{bulk}}$ |
| | | | $R_{\text{Auger_li_n}} \approx C_n^* N_D W_{\text{bulk}} pn$ | Bulk (n) | $J_{0\ \text{Auger_li_n}} = qC_n^* N_D n_i^2 W_{\text{bulk}}$ |
| | | SRH Rec. in low injection | $R_{\text{SRH_li_p}} \approx \frac{W_{\text{bulk}}}{\tau_n N_A} pn$ | Bulk(p) | $J_{0\ \text{SRH_li_p}} = \frac{qn_i^2 W_{\text{bulk}}}{\tau_n N_A}$ |
| | | | $R_{\text{SRH_li_n}} \approx \frac{W_{\text{bulk}}}{\tau_p N_D} pn$ | Bulk (n) | $J_{0\ \text{SRH_li_n}} = \frac{qn_i^2 W_{\text{bulk}}}{\tau_p N_D}$ |
| | | Surface Rec. (surface SRH rec., complex) | $R_{\text{surf}} \approx S \cdot \Delta n; \text{ or } \approx J_{0\ \text{surf}} \left(\frac{pn}{qn_i^2} \right)$ | Surface | $J_{0\ \text{surf_li_p+}} = qS n_{N_A^*}^{\frac{n_i^2}{n_A}}$ $J_{0\ \text{surf_li_n+}} = qS p_{N_D^*}^{\frac{n_i^2}{n_D}}$, or J_{0E} |
| $\approx R_{02} \left(\frac{pn}{n_i^2} \right)^{1/2}$ | 2 | SRH Rec. in high injection | $R_{\text{SRH_hi}} = \frac{W_{\text{bulk}}}{\tau_n + \tau_p} \Delta n$ | Bulk | $J_{0\ \text{SRH_hi}} = \frac{qn_i W_{\text{bulk}}}{\tau_n + \tau_p}$ |
| | | SRH Rec. at depletion region | $R_{\text{DR}} \approx \int_{\text{DR}} \frac{(n(x)p(x) - n_i^2)}{\tau_{p0}n(x) + \tau_{n0}p(x)} dx$ | Depletion region | $\approx J_{01.85}$ |
| | | SRH Rec. at edge region | $R_{\text{surf}} \approx S \cdot \Delta n; \text{ or } \approx J_{0\ \text{surf}} \left(\frac{pn}{q^2 n_i^2} \right)^{1/2}$ | Edge of p-n junction | $J_{0\ \text{surf_hi}} = qS n_i$ |

$$\Delta n_s \approx \frac{np}{p_s} \approx \frac{(N_D + \Delta n)}{(N_{A+} + \Delta n_s)} \Delta n \quad (7)$$

and

$$S_{\text{eff}} \approx \frac{(N_D + \Delta n)}{(N_{A+} + \Delta n_s)} S \quad (8)$$

where N_{A+} and N_D are the effective doping concentration at surface and doping concentration in bulk, respectively. Here, S represents the S_{it} in Figure 5.

Figure 5d shows the S_{eff} as a function of Δn (defined by Equation 8), where N_{A+} changes from 10^{13} to 10^{19} cm^{-3} , while N_D and S are set as $3 \times 10^{15} \text{ cm}^{-3}$ and 1 cm/s , respectively. When $N_{A+} = N_D$ (green line), similar as the situation without surface field (i.e., flat band), there are $S_{\text{eff}} = 1 \text{ cm/s}$ at low injection and $S_{\text{eff}} = 0.5 \text{ cm/s}$ at high injection. This is consistent with the general law of SRH recombination. When $N_{A+} < N_D$, the S_{eff} appears even above the original S at low injection ($\Delta n \ll N_D$). For the case of sufficiently high surface doping, that is, $N_{A+} > N_D$, it is divided into three stages. In the first stage, at $\Delta n \ll N_D$, the $S_{\text{eff}} = (N_D/N_{A+})S$ relationship is established, where S_{eff} basically maintains a fixed value with the change of Δn and decreases with the increase of N_{A+} , indicating that a larger field leads to a smaller surface recombination rate. In the second stage of $N_D \ll \Delta n \ll N_{A+}$, the $S_{\text{eff}} = [(N_D + \Delta n)/N_{A+}]S$ relationship is established, indicating that the S_{eff} increases with Δn . In the third stage, at $\Delta n \gg N_{A+}$, the surface field of φ_s is almost equal to 0, and thus, the

surface recombination returns to the field-absent-case, that is, 0.5 cm/s here.

In general, the relationship between the S_{eff} and Δn is complex as shown in Figure 5d. However, because the surface recombination can also be classified as SRH recombination, the U_s/W_{bulk} as a function of iV_{OC} is similar as Figure 3a. When the field is sufficiently strong, such as $N_{A+} > 3 \times 10^{18} \text{ cm}^{-3}$, for $S = 1 \text{ cm/s}$, the corresponding J-V relationship in the range of $V_{\text{MPP}}-V_{\text{OC}}$ can be described as the diode equation of J_{01} , that is, $J_{01\ \text{surf}} = \frac{n_i^2}{N_{A+}} qS$ (for p+n junction). When the field is weak, such as $N_{A+} < 3 \times 10^{14} \text{ cm}^{-3}$, for $S = 1 \text{ cm/s}$, the corresponding J-V relationship in the range of $V_{\text{MPP}}-V_{\text{OC}}$ can be described as the diode equation of J_{02} , that is, $J_{02\ \text{surf}} = n_i qS$ (for p+n junction).

Table 2 summarizes the formulas for the abovementioned recombination processes in separate high and low injections. The spatial distribution of J_{01} , J_{02} , and $J_{0\ 2/3}$ in silicon solar cell is displayed in Figure 6. The expressions of the recombination saturation current density (J_{0m} , m is the ideality factor) are also defined. For example, when $m = 2/3$, the recombination current density is only related to the high injection of Auger recombination, the relationship with Δn is the third power, and the reverse saturation current $J_{0\ \text{Auger_hi}}$ (i.e., $J_{0\ 2/3\ \text{Auger}}$) is proportional to the thickness of silicon wafer (W_{bulk}). In other words, a thinner silicon wafer can effectively reduce the influence of Auger recombination from bulk on cell PCE. For $m = 1$, almost all the recombination is linked to low injection. While J_{02} recombination current density mainly comes from the SRH recombination of bulk silicon at high injection (especially in the wafer with low N_D), depletion regions and edge regions (more details are showed in

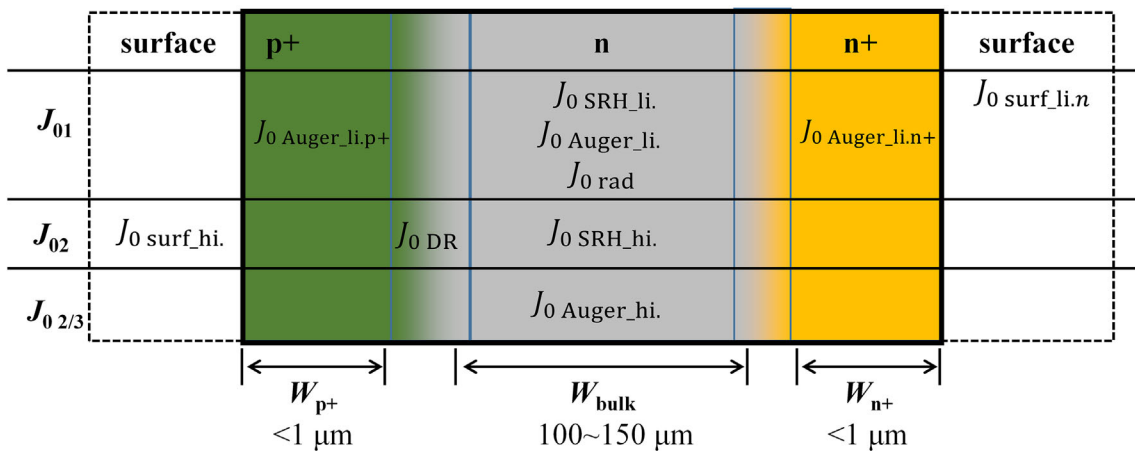


FIGURE 6 The distribution of J_{01} , J_{02} , and $J_{0\ 2/3}$ in silicon solar cell.

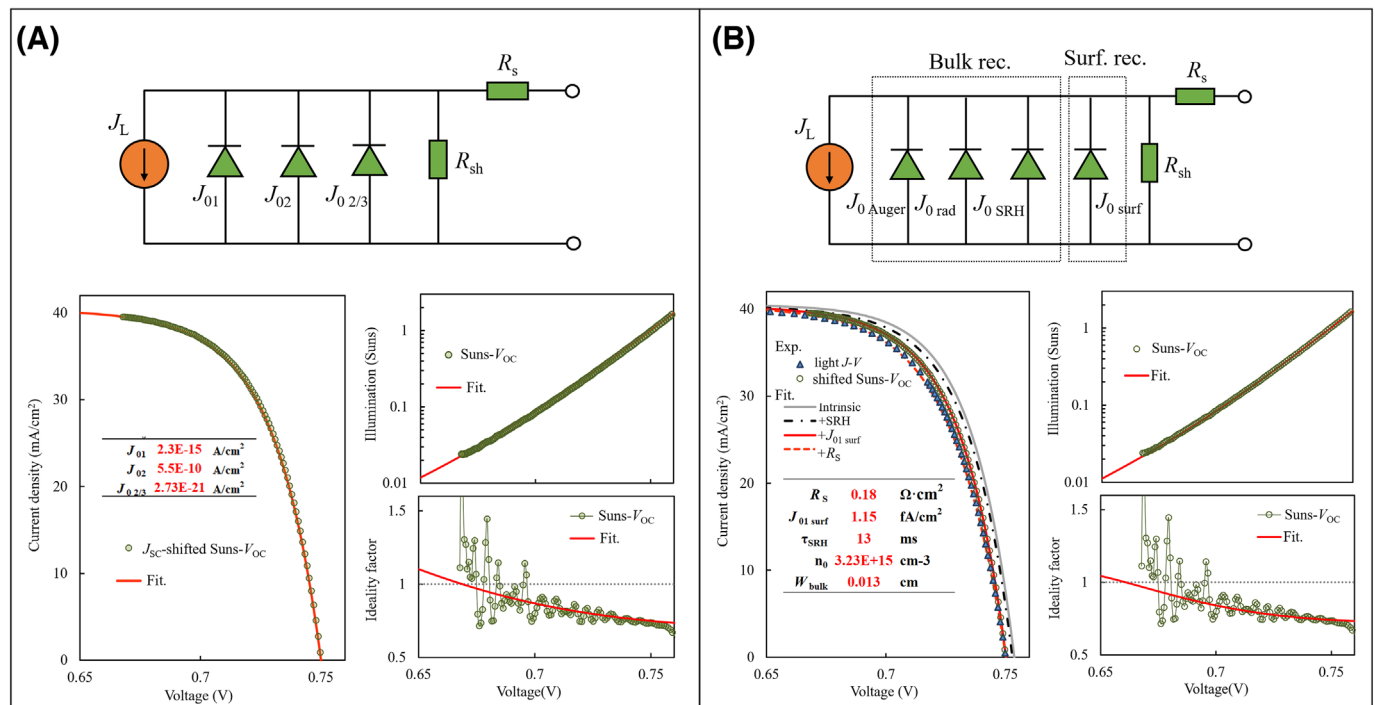


FIGURE 7 Fitting of J-V curves by the triple-diode equivalent model and our simplified recombination model. (a) Triple-diode model. It utilizes J_{01} , J_{02} , and $J_{0\ 2/3}$ diodes to fit the experimental J-V curves extracted by $Suns-V_{OC}$ (green circle). The red color lines are the fitting curves. (b) Simplified recombination model. It utilizes the equations of intrinsic, SRH, and surface recombination to fit the J-V curves extracted by $Suns-V_{OC}$ (green circle) and the R_s equation to fit the light J-V curves (blue triangle), where the J-V curves include three forms of expression, that is, light J-V curve (with liner y-axis), illumination-voltage curve (as dark J-V curves with logarithmic y-axis), and m-V curve. The “intrinsic,” “+SRH,” “+ $J_{01\ surf}$,” and “+ R_s ” mean that the J-V curves adding intrinsic recombination (including Auger recombination and radiative recombination with photon recycling), SRH recombination, surface recombination ($J_{01\ surf}$ including $J_{01\ surf}$ and $J_{02\ surf}$), and series resistance (R_s) equations one by one.

| | Recombination | $J_{01}\ (\text{A}/\text{cm}^2)$ | $J_{02}\ (\text{A}/\text{cm}^2)$ | $J_{0\ 2/3}\ (\text{A}/\text{cm}^2)$ |
|----------------|---------------|----------------------------------|----------------------------------|--------------------------------------|
| Bulk | Radiative | 3.02×10^{-16} | | |
| | Auger | 7.11×10^{-16} | | 2.7×10^{-21} |
| | SRH | 3.78×10^{-15} | 6.98×10^{-10} | |
| $J_{01\ surf}$ | SRH | 1.15×10^{-15} | | |

TABLE 3 The calculated parameters of J_{01} , J_{02} , and $J_{0\ 2/3}$ according to the fitting parameters in Figure 7b and the formulas in Table 2.

Figure S6). Based on above partitioning and simplified formula, one can quickly calculate the general current equation through the recombination current equation with J_{01} , J_{02} , and $J_{0\ 2/3}$.

6 | APPLICATIONS OF THE TRIPLE-DIODE EQUIVALENT MODEL AND SIMPLIFIED RECOMBINATION MODEL IN J-V CURVE ANALYSIS

The experimental J-V curve can be fitted through a triple-diodes equivalent circuit with J_{01} , J_{02} , and $J_{0\ 2/3}$ (Figure 7a), as well as by the simplified recombination model (Figure 7b). The upper panels in Figure 7a,b show the corresponding equivalent circuits. The triple-diode model uses only three parameters of J_{01} , J_{02} , and $J_{0\ 2/3}$ to describe the recombination and corresponding performance of solar cell. The simplified recombination model can not only distinguish the sources and types of recombination but also distinguish the recombination from intrinsic recombination, bulk SRH recombination, and surface recombination ($J_{01\ surf}$ and $J_{02\ surf}$, here, $J_{02\ surf}$ is negligible) equations in sequence. Similar as the Figure 1c-e, three typical J-V curves, that is, light J-V curve (similar as the J-V curves with liner ordinate in Figure 1c), illumination-voltage curve (i.e., Suns- V_{OC} curve, similar as the J-V curves with logarithmic ordinate in Figure 1d, where $J = J_{SC}\cdot\text{Suns}$), and ideality factor-voltage ($m\cdot V$) curve, are taken for evaluation on the effectiveness of these two modes. The blue triangle and green circle represent the experimental data of light J-V curve and Suns- V_{OC} curve, respectively, while the red solid line is the fitted line of recombination current density ($J_{rec.}$) calculated by the equation of

$$J_{rec.} = \sum_{m=1,2,2/3} J_{0m} \left[\exp\left(\frac{V}{m \cdot V_T}\right) - 1 \right] \quad (9)$$

for triple-diode model, and

$$J_{rec.} = (U_{Auger} + U_{rad} + U_{SRH})qW_{bulk} + \sum_{m=1,2} J_{0m\ surf.} \left[\exp\left(\frac{V}{m \cdot V_T}\right) - 1 \right] \quad (10)$$

for simplified recombination model.

To fulfill our simplified recombination model, the fitting process must follow the subsequent steps. Firstly, upon the already known silicon wafer characteristics, such as doping concentration, thickness, and quality (i.e., τ_{SRH}), the corresponding recombination formula (or Table 2) is employed to calculate the respective J-V curve related to bulk recombination. Then, the experimental lines of illumination-voltage and ideality factor-voltage data are fitted through adjusting J_{01} and J_{02} (see bottom right panels in Figure 7a,b). At last, the experimental light J-V curves are fitted through adjusting R_s . It should be noted that, in simplified recombination model, the set of silicon wafer quality will directly impact the J_{01} (or J_{02}) ratio between the surface recombination and bulk recombination, so the silicon

wafer quality should be assessed by separate passivation test if necessary.

The fitting J-V curve (gray solid line) in Figure 7b contains the Auger recombination (by Black and Macdonald¹²) and the radiative recombination with a photon recycling of ~ 0.6 , while U_{SRH} is according to equation in Table 1. From the comparison between the three J-V curves, one can see that both methods are quite effective in fitting the experimental curve. In fact, according to the description in Table 2, though the m of bulk recombination will change with injection, the J_0 at low/high injection can still be calculated (Table 3). From the triple-diode model, J_{01} , J_{02} , and $J_{0\ 2/3}$ are $2.3\text{ fA}\cdot\text{cm}^{-2}$, $5.5 \times 10^{-10}\text{ A}\cdot\text{cm}^{-2}$, and $2.73 \times 10^{-21}\text{ A}\cdot\text{cm}^{-2}$, respectively, which are nearly equal to the results of that in Table 3 (simplified recombination model), that is, $J_{01\ rad} + J_{01\ Auger} + J_{01\ surf} = 2.27\text{ fA}/\text{cm}^2$, $J_{02\ SRH} = 7.0 \times 10^{-10}\text{ A}\cdot\text{cm}^{-2}$, and $J_{0\ 2/3\ Auger} = 2.73 \times 10^{-21}\text{ A}\cdot\text{cm}^{-2}$, indicating the equivalence of the two methods. Uniquely, the latter can better quantify various type of recombination, especially when the information of silicon bulk are measurable, which is very suitable for process development and loss analysis for solar cells.

7 | FORECASTING THE IMPLIED FF (IFF) OF SILICON SOLAR CELLS VIA SIMPLIFIED RECOMBINATION MODEL

At a condition of low edge recombination and depletion region recombination (Figure S6), the main sources of J_{02} can be basically ignored here, and the FF and V_{OC} will be mainly affected by $J_{01\ surf}$ and τ_{SRH} . Figure 8 shows the iV_{OC} or iFF as the function of τ_{SRH} and $J_{01\ surf}$. The corresponding fitting conditions are shown in the upper left corner in Figure 8a. It can be clearly seen that, after setting the parameters of silicon wafers and the photocurrent (J_L), along with the decrease of $J_{01\ surf}$ and the increase of τ_{SRH} , the iV_{OC} increase will slow down, especially when 746 mV is reached. This indicates that the intrinsic recombination is gradually playing a dominant role. At this time, the promotion of iFF will become as a main driving force for efficiency growth. In the range of $\tau_{SRH} < 10\text{ ms}$ and $J_{01\ surf} < 1\text{ fA}/\text{cm}^2$, iFF ramps up significantly with the increase of τ_{SRH} , but not $J_{01\ surf}$. The bulk SRH recombination become the main source of recombination at this time. As the $\tau_{SRH} > 20\text{ ms}$ and $J_{01\ surf} > 1\text{ fA}/\text{cm}^2$, the surface recombination will become the main source of recombination.

For our SHJ solar cells,¹¹ the corresponding total $J_{01\ surf}$ can be suppressed down to $2\text{ fA}/\text{cm}^2$, and even to below $1\text{ fA}/\text{cm}^2$ in excellent cases. In this case, wafer quality will undoubtedly have a great effect on the cell efficiency. In addition, it can be seen from the figure that if the corresponding iV_{OC} and iFF can be tested, the wafer quality and surface passivation quality corresponding to the cells can be roughly estimated (any additional J_{02} information ignored here can be contained in τ_{SRH}). The parameters of the 26.3%-PCE SHJ solar cell showed in Figure 1 are marked in Figure 8 by yellow star, where the corresponding J_{01} and τ_{SRH} are attained by fitting the corresponding J-V curves. Obviously, if $J_{01\ surf} < 0.8\text{ fA}/\text{cm}^2$, and τ_{SRH} can be raised to $> 30\text{ ms}$, its iFF will exceed 88%.

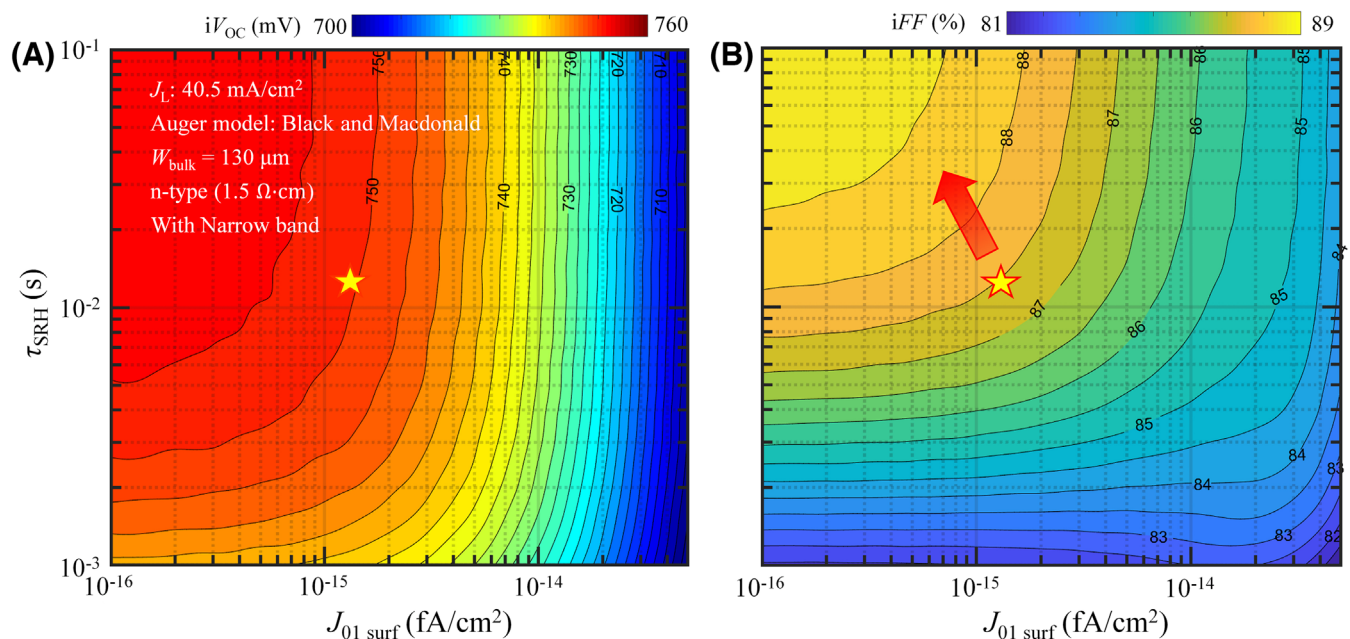


FIGURE 8 Forecasts on the iV_{OC} and iFF of silicon solar cells. (a) The iV_{OC} as a function of τ_{SRH} and $J_{01\ surf}$. (b) The iFF as a function of τ_{SRH} and $J_{01\ surf}$. The red star represents the 86.59%-FF solar cell in Figure 1b–e. The real FF = pFF – ΔFF , where $\Delta FF \approx R_s \times 5\text{ (%}\cdot\Omega^{-1}\cdot\text{cm}^{-2}\text{)}$ (unit of R_s is $\Omega\cdot\text{cm}^2$) according to the ref.,¹⁶ and pFF ≈ iFF when shunt resistance is high enough. The pFF is pseudo FF, which consider the recombination and shunt influence, while iFF is implied FF, which only consider the recombination effect.

It is noted that the abovementioned iFF only consider the recombination effect. In fact, the practical FF should also need to consider the influence of series resistance (R_s) and shunt resistance (R_{sh}) of solar cells. If R_{sh} is high enough, pFF ≈ iFF, where pFF is pseudo FF in which the influence from both recombination and R_{sh} are considered. According to the relationship of $\Delta FF \approx R_s \times 5\%$ (unit of R_s is $\Omega\cdot\text{cm}^2$),¹⁵ the practical FF can be deduced from pFF. For example, the 26.30% efficient cell demonstrates a series resistance of $\sim 0.2\text{ }\Omega\cdot\text{cm}^2$, where accordingly its FF can be calculated as $pFF - \Delta FF \approx 87.41\% - 0.2 \times 5\% = 86.41\%$. The calculated value is consistent with the measured value in decent accuracy.

Further reduction on SRH recombination to increase τ_{SRH} turns to be an effective means to further improve iFF. If keeping the same R_s , through improving τ_{SRH} to 30 ms and reducing $J_{01\ surf}$ to 0.8 fA/cm^2 , FF can approach 87.4% (88.4% – 0.2 × 5%). Further improving τ_{SRH} to 90 ms and reducing $J_{01\ surf}$ to 0.7 fA/cm^2 , FF can approach 88.0% (89.0% – 0.2 × 5%).

8 | CONCLUSION

Thanks to the advances in silicon PV technologies in passivation and resistance reduction, record filling factor of silicon solar cells has reached 86.6%. The corresponding light J-V curve showed an average ideality factor less than 1 between MPP and open-circuit conditions. By using a double-diode model with $J_{02/3}$ and J_{01} , representing intrinsic recombination and surface recombination, the process occurring in the rapid increments of FF with J_{01} reduction experimentally observed

can be completely reproduced. Furthermore, the relationship between ideality factor and specific recombination process is established. For surface recombination with a strong field, the J-V curves show the characteristics of J_{01} diode. It is also revealed that J_{02} mainly comes from the depletion region and the edge region of p-n junction. Then we discriminated the recombination current density of J_0 in specific regions and established the relation between triple-diode model and our simplified recombination mode. Both models were compared to fit measured J-V curves, and their equivalence was demonstrated. Finally, we show that continuous improving bulk quality (τ_{SRH}) and surface recombination (J_{01}) will lead to further promotion of FF. The estimated FF can approach 88.0% when $\tau_{SRH} \geq 90\text{ ms}$, $J_{01\ surf} \leq 0.7\text{ fA/cm}^2$, and $R_s \leq 0.2\text{ }\Omega\cdot\text{cm}^2$.

ACKNOWLEDGMENTS

This work was financially supported by the National Key Research and Development Program of China (2022YFB4200203) and the National Natural Science Foundation of China (62034009, 62104268), Shenzhen Fundamental Research Program (JCYJ20200109142425294), and Guangdong Basic and Applied Basic Research Foundation (2019B151502053).

CONFLICT OF INTEREST STATEMENT

The authors declare no competing interests.

DATA AVAILABILITY STATEMENT

The data that support the findings of this study are available from the corresponding author upon reasonable request.

REFERENCES

1. Cuevas A, Macdonald D. Measuring and interpreting the lifetime of silicon wafers. *Solar Energy*. 2004;76(1-3):255-262. doi:[10.1016/j.solener.2003.07.033](https://doi.org/10.1016/j.solener.2003.07.033)
2. Brendel R, Peibst R. Contact selectivity and efficiency in crystalline silicon photovoltaics. *IEEE J Photovolt*. 2016;6(6):1413-1420. doi:[10.1109/JPHOTOV.2016.2598267](https://doi.org/10.1109/JPHOTOV.2016.2598267)
3. Brendel R, Riencker M, Peibst R. A quantitative measure for the carrier selectivity of contacts to solar cells. 32nd European Photovoltaic Solar Energy Conference & Exhibition. 2016.
4. Chan DSH, Phang JCH. Analytical methods for the extraction of solar-cell single- and double-diode model parameters from I-V characteristics. *IEEE Trans Electron Devices*. 1987;34(2):286-293. doi:[10.1109/T-ED.1987.22920](https://doi.org/10.1109/T-ED.1987.22920)
5. <http://www.griddlersolar.com>
6. Macdonald DH. *Recombination and Trapping in Multicrystalline Silicon Solar Cells*. Australian National University; 2001.
7. Richter A, Hermle M, Glunz SW. Reassessment of the limiting efficiency for crystalline silicon solar cells. *IEEE J Photovolt*. 2013;3(4):1184-1191. doi:[10.1109/JPHOTOV.2013.2270351](https://doi.org/10.1109/JPHOTOV.2013.2270351)
8. Razzap A, Allen T, Wolf A. Design criteria for silicon solar cells with fill factors approaching the Auger limit. *ACS Energy Lett*. 2023;8(10):4438-4440. doi:[10.1021/acsenergylett.3c01519](https://doi.org/10.1021/acsenergylett.3c01519)
9. Green MA. Solar cell fill factors: general graph and empirical expressions. *Solid-State Electron*. 1981;24(8):788-789. doi:[10.1016/0038-1101\(81\)90062-9](https://doi.org/10.1016/0038-1101(81)90062-9)
10. Allen TG, Bullock J, Yang X, Javey A, Wolf SD. Passivating contacts for crystalline silicon solar cells. *Nat Energy*. 2019;4(11):914-928. doi:[10.1038/s41560-019-0463-6](https://doi.org/10.1038/s41560-019-0463-6)
11. Lin H, Yang M, Ru X, et al. Silicon heterojunction solar cells with up to 26.81% efficiency achieved by electrically optimized nanocrystalline-silicon hole contact layers. *Nat Energy*. 2023;8(8):789-799. doi:[10.1038/s41560-023-01255-2](https://doi.org/10.1038/s41560-023-01255-2)
12. Black LE, Macdonald DH. On the quantification of Auger recombination in crystalline silicon. *Solar Energy Mater Solar Cells*. 2022;234:111428. doi:[10.1016/j.solmat.2021.111428](https://doi.org/10.1016/j.solmat.2021.111428)
13. Richter A, Werner F, Cuevas A, Schmidt J, Glunz SW. Improved quantitative description of Auger recombination in crystalline silicon. *Phys Rev B*. 2012;86(16):165202. doi:[10.1103/PhysRevB.86.165202](https://doi.org/10.1103/PhysRevB.86.165202)
14. McIntosh, K.R. Lumps, humps and bumps: three detrimental effects in the current-voltage curve of silicon solar cells. University of New South Wales (2001).
15. Cuevas A. The recombination parameter J_0 . *Energy Procedia*. 2014;55:53-62. doi:[10.1016/j.egypro.2014.08.073](https://doi.org/10.1016/j.egypro.2014.08.073)
16. Pysch D, Mette A, Glunz SW. A review and comparison of different methods to determine the series resistance of solar cells. *Solar Energy Mater Solar Cells*. 2007;91(18):1698-1706. doi:[10.1016/j.solmat.2007.05.026](https://doi.org/10.1016/j.solmat.2007.05.026)

SUPPORTING INFORMATION

Additional supporting information can be found online in the Supporting Information section at the end of this article.

How to cite this article: Lin H, Wang G, Su Q, et al. Unveiling the mechanism of attaining high fill factor in silicon solar cells. *Prog Photovolt Res Appl*. 2024;32(6):359-371. doi:[10.1002/pip.3775](https://doi.org/10.1002/pip.3775)